WATER RESEARCH 60 (2014) 267–277

Available online at www.sciencedirect.com

ScienceDirect

journal homepage: www.elsevier.com/locate/watres

Clarifying the regulation of NO/N_2O production in *Nitrosomonas europaea* during anoxic–oxic transition via flux balance analysis of a metabolic network model

Octavio Perez-Garcia [a], *Silas G. Villas-Boas* [b], *Simon Swift* [c], *Kartik Chandran* [d], *Naresh Singhal* [a,*]

[a] *Department of Civil and Environmental Engineering, The University of Auckland, Private Bag 92019, Auckland 1142, New Zealand*

[b] *Centre for Microbial Innovation, School of Biological Sciences, The University of Auckland, Private Bag 92019, Auckland 1142, New Zealand*

[c] *Department of Molecular Medicine and Pathology, The University of Auckland, Private Bag 92019, Auckland 1142, New Zealand*

[d] *Department of Earth and Environmental Engineering, Columbia University, 500 West 120 Street, New York, USA*

ARTICLE INFO

Article history:
Received 31 December 2013
Received in revised form
2 April 2014
Accepted 30 April 2014
Available online 14 May 2014

Keywords:
Nitrous oxide production
Ammonia oxidizing bacteria
Nitrosomonas europaea metabolism
Metabolic network modelling
Flux balance analysis
Nitrifier denitrification

ABSTRACT

The metabolic mechanism regulating the production of nitric and nitrous oxide (NO, N_2O) in ammonia oxidizing bacteria (AOB) was characterized by flux balance analysis (FBA) of a stoichiometric metabolic network (SMN) model. The SMN model was created using 51 reactions and 44 metabolites of the energy metabolism in *Nitrosomonas europaea*, a widely studied AOB. FBA of model simulations provided estimates for reaction rates and yield ratios of intermediate metabolites, substrates, and products. These estimates matched well, deviating on average by 15% from values for 17 M yield ratios reported for non-limiting oxygen and ammonium concentrations. A sensitivity analysis indicated that the reactions catalysed by cytochromes aa3 and P460 principally regulate the pathways of NO and N_2O production (hydroxylamine oxidoreductase mediated and nitrifier denitrification). FBA of simulated *N. europaea* exposure to oxic–anoxic–oxic transition indicated that NO and N_2O production primarily resulted from an intracellular imbalance between the production and consumption of electron equivalents during NH_3 oxidation, and that NO and N_2O are emitted when the sum of their production rates is greater than half the rate of NO oxidation by cytochrome P460.

* *Corresponding author*. Tel.: +64 9 923 4512.
E-mail addresses: n.singhal@auckland.ac.nz, nsin024@gmail.com (N. Singhal).

http://dx.doi.org/10.1016/j.watres.2014.04.049
0043-1354/

1. Introduction

Ammonia oxidizing bacteria (AOB) produce nitric and nitrous oxide (NO and N_2O) during nitrification and autotrophic denitrification in wastewater treatment processes (Ahn et al., 2010; Foley et al., 2010; Kampschreur et al., 2009). A survey of wastewater treatment plants in the US showed that aerobic zones generally contributed more to N_2O fluxes than anoxic zones from BNR reactors (Ahn et al., 2010); the N_2O emission fraction ranges between 0 and 25% of the influent N-load according to the International Panel for Climate Change (IPCC) (Kampschreur et al., 2009). N_2O emissions contribute to ozone depletion and its global warming potential is ~300 times higher than that of CO_2 on a per molecule basis (Ravishankara et al., 2009; Wuebbles, 2009). The operational conditions of wastewater treatment processes that lead to NO and N_2O production by AOB are related to changes in the concentration of electron donors (NH_4^+ and NH_2OH) and acceptors (O_2 and NO_2^-) (Chandran et al., 2011; Kampschreur et al., 2008). However, despite the availability of extensive information on nitrogen respiration and energy production in AOB, the metabolic triggers and regulatory mechanisms controlling NO and N_2O production are not well understood.

NO/N_2O production in AOB occurs via two pathways: (i) the aerobic hydroxylamine oxidation pathway mediated by hydroxylamine oxidoreductase (HAO) and (ii) the nitrifier denitrification pathway mediated by nitrite reductase (NIR) and nitric oxide reductase (NOR) enzymes (Cabail and Pacheco, 2003; Stein, 2010, 2011; Wunderlin et al., 2012). From pure cultures of *Nitrosomonas europaea*, a model AOB species that has been abundantly detected in full scale nitrification processes (Wagner et al., 2002), it is known that these two pathways are part of nitrogen respiration, electron transport chain, and energy generation mechanisms of AOB (Whittaker et al., 2000; Yu et al., 2010). As a result, activation of the HAO mediated pathway leads to generation of electron equivalents and activation of the NIR mediated pathways implies a consumption of electron equivalents. However, details of how the availability of electron donors (NH_4^+ or NH_2OH) and acceptors (O_2 or NO_2^-) influences the activity of these pathways remain unclear.

Activated Sludge (ASM) models have been modified to dynamically predict NO and N_2O production under different environmental conditions by linking NO and N_2O production to the respiratory activity and the responsible metabolic pathway (Kampschreur et al., 2007; Ni et al., 2011, 2013; Pan et al., 2013; Yu et al., 2010). This approach however does not clarify why these gases are produced, as NO and N_2O production has largely been described as being decoupled from the cell's energy metabolism. Furthermore, different routes for production or consumption of electron equivalents are ignored. A different approach taken by Wunderlin et al. (2013) involving the use of isotope signatures of N_2O produced by mixed microbial populations could quantify the contribution of each of the two N_2O production pathways under different environmental conditions. However, the method provides no explanation for what activated the dominant pathway. Added to this, the difficulty and expense of such isotopic signature based experiments could limit their wide adoption in understanding the behaviour of laboratory or full scale systems.

Stoichiometric metabolic network (SMN) modelling and flux balance analysis (FBA) are emerging techniques in systems biology that could be used to quantify the rate of reactions within the network formed by chemical compounds and sequenced chemical reactions in cells' metabolism (Durot et al., 2009; Oberhardt et al., 2009; Orth et al., 2010). FBA provides a 'snapshot' estimation of reaction rates in the metabolic network at a specific metabolic steady state (Orth et al., 2010), and we use it to quantify the simultaneous activity in the hydroxylamine mediated and nitrifier denitrification pathways during NO and N_2O production by AOB. In this study *Nitrosomonas europaea* served as a model AOB as its metabolism as well as the pathways for ammonium oxidation and production of energy, NO and N_2O, are known (Poughon et al., 2001; Sayavedra-Soto and Arp, 2011; Stein, 2010). Furthermore, its genome has been sequenced, which allows the reconstruction of its entire complement of metabolic pathways (Chain et al., 2003). We construct a SMN model based on *Nitrosomonas europaea* energy production metabolism and enzymology, and use it in combination with FBA to quantify the metabolic rates of NO and N_2O production pathways during oxic–anoxic–oxic transitions of *N. europaea* cultures. The obtained metabolic rates are used to infer the physiological mechanisms responsible for regulation of pathways leading to the production of these gases.

2. Materials and methods

2.1. Metabolic network development

A metabolic network model for biochemical reactions and metabolites formed during *N. europaea* energy production metabolism was constructed by following the procedure described by Thiele and Palsson (2010) and using organism-specific genomic and biochemical information from literature (references in Table S1 of Supporting Information (SI)) and the metabolic pathway databases KEGG and MetaCyc (respectively accessible at http://www.genome.jp/kegg/ and http://metacyc.org/). The network consists of mass and charge balanced stoichiometric biochemical reactions that are classified as either reversible or irreversible (Savinell and Palsson, 1992; Thiele and Palsson, 2010).

The reactions for energy production in *N. europaea* cells are modelled as occurring in three cell compartments: extracellular, periplasmic and cytoplasmic spaces (Chain et al., 2003); labels [e], [p] and [c] have respectively been assigned to metabolic compounds to indicate their occurrence in extracellular, periplasmic and cytoplasmic compartments (Fig. 1A). The metabolite NH_4^+[e] is thereby differentiated from NH_4^+[p] and the exchange between extracellular and periplasmic spaces can be simulated as NH_4^+[e] $\leftrightarrow$ NH_4^+[p]. Further information about network compartmentalization can be found in Thiele and Palsson (2010). The constructed AOB-SMN model consists of 44 metabolites and 49 stoichiometric reactions categorized as follows: 11 exchange reactions representing the flow of metabolic compounds in and out of the cell (IDs of

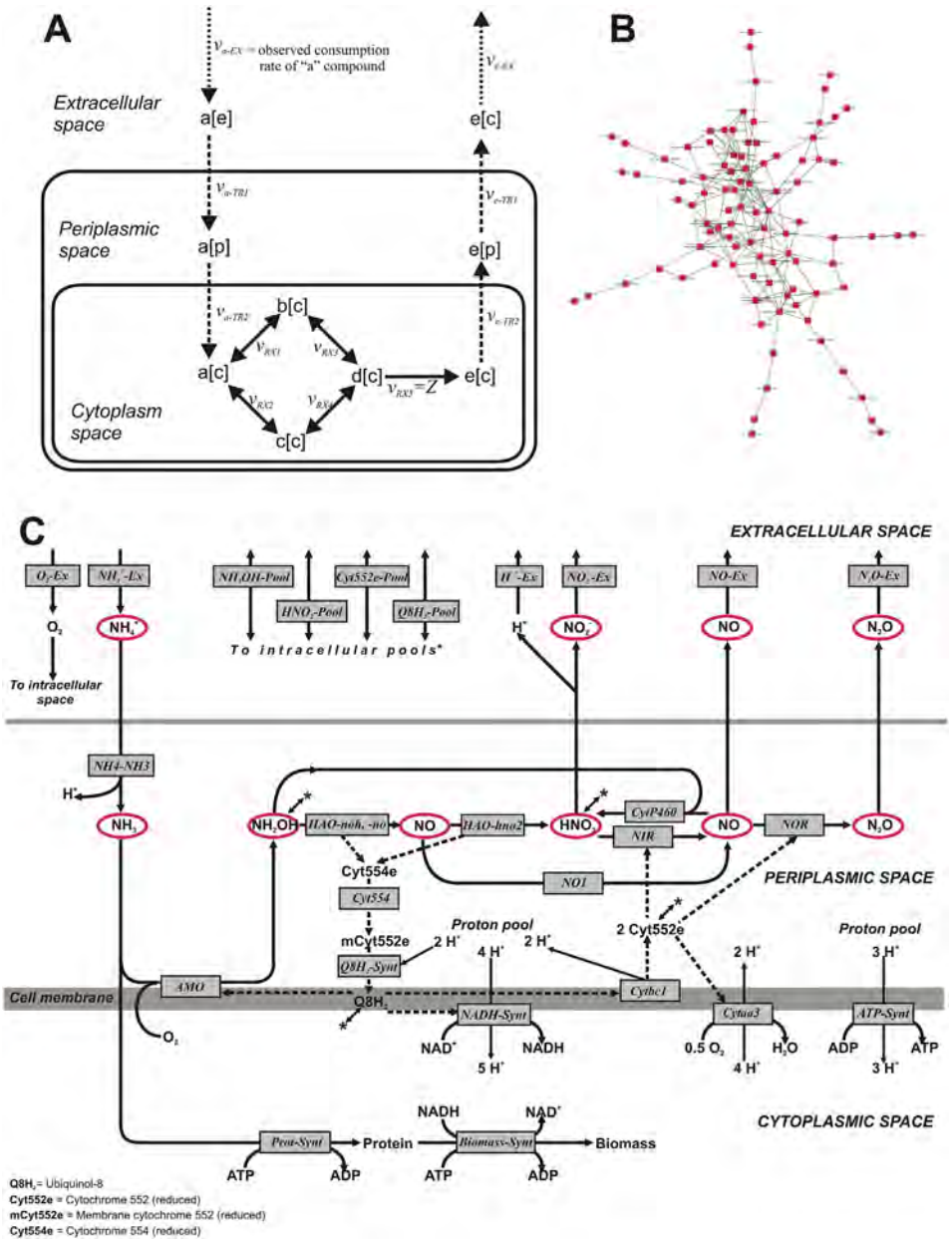

Fig. 1 – The SMN-AOB model developed in this study: (A) The conceptual scheme of FBA in the metabolic network. Metabolites "a" to "e" are shown in extracellular, periplasmic, or cytoplasmic compartments using labels [e], [p] or [c]; doted, dashed and solid arrows respectively represent exchange, transport/diffusion, and metabolic reactions. (B) Visualization of the SMN-AOB model created using Cytoscape in which nodes represent reactions as well as metabolites. (C) Schematic representation of reactions and metabolic compounds considered in the AOB-SMN model. Black arrows represent metabolic reactions with their ID name shown in grey boxes and dashed lines represent the pathways of electron exchange. Ovals show the main nitrogenous compounds. Full reaction equations and the list of metabolic compounds are presented in Tables S1 and S2 of SI.

these reactions have the extension "-*Ex*"), 4 reactions representing the consumption and production of metabolic compounds from intracellular pools (IDs of these reactions have the extension "-*Pool*"), 17 reactions representing the transport or diffusion of metabolic compounds between compartments [e], [p] and [c], 14 reactions for *N. europaea* energy production metabolism catalysed by enzymes, including ammonia respiration, NO and N_2O production, and energy production, and 3 biomass synthesis reactions (all reaction IDs are showed with italicized text). The network formed by these reactions and metabolites, produced with Cytoscape 3.0.1 software (Cytoscape consortium, San Diego, USA), is shown in Fig. 1B where nodes represent reactions and metabolites; the external branches are the 11 exchange reactions; and the most highly connected nodes are lumped in the central region of the network.

A scheme of the primary reactions and metabolites considered in the model is illustrated in Fig. 1C, as follows: exchange of compounds between cellular and extracellular spaces, oxidation and reduction of nitrogenous compounds in the periplasmic space, and protein and biomass synthesis in the cytoplasmic space, along with the electron transport chain. The hydroxylamine oxidoreductase (HAO) mediated NO/N_2O production pathway involves oxidative NOH and NO production by HAO (Kostera et al., 2008) (reactions IDs: *HAO-noh*, *HAO-no*, and *NO1*), and the subsequent reduction of NO to N_2O by nitric oxide reductase (NOR) (reactions ID: *NOR*). The nitrifier denitrification NO/N_2O production pathway uses HNO_2 and NO as final electron acceptors in two reduction reactions (*NIR* and *NOR*). Ubiquinol-8 ($Q8H_2$) and reduced cytochrome 552 (Cyt552e) play a particularly significant role in the modelled electron transport chain by acting as pivot compounds that distribute the flow of electrons to different electron acceptors (Fig. 1C). Details of the genome and biochemical information used to assemble the metabolic network are presented in the Supporting Information (SI). Table S1 of SI presents a list of model's primary metabolic reactions, their stoichiometric equations, the associated reaction's catalyst enzyme and associated references and Table S2 of SI lists model's metabolic compounds.

2.2. FBA Model simulations

FBA simulations were performed by mathematically representing the reconstructed SMN using the COBRA toolbox 2.0 (Schellenberger et al., 2011; The open COBRA project, San Diego, USA) working with the linear programming solver GLPK (GNU project, Moscow, Russia) within Matlab® 7 R2010b (The Mathworks Inc, Massachusetts, USA). The different methods in COBRA toolbox 2.0 that were used for network evaluation, debugging and simulation are listed in Table S3 of SI. FBA was applied to estimate the unknown rates of network reactions by using values of consumption rates of substrates (i.e. oxygen and ammonium) as model input. The unknown rates (or fluxes) were found by optimizing an objective function (Z) subject to the specified substrate uptake rates (Becker et al., 2007; Orth et al., 2010; Varma and Palsson, 1994). FBA can be mathematically expressed as:

$$S * v = 0 = \frac{dX}{dt} \quad (1)$$

where S is a stoichiometric matrix of *m* metabolites (rows) and *n* reactions (columns), with s_{ij} representing stoichiometric coefficient for *i*th metabolite participating in *j*th reaction; *v* is a vector of *n* reaction rates v_j that are estimated by optimizing within constraints so that $\propto_j \leq v_j \leq \beta_j$, where $\propto_j$ and β_j represent the lower and upper bounds for reaction rate v_j; *X* represents the concentration of metabolites, and *t* is time.

Transients in metabolism are typically on the order of a few minutes, and metabolic transients are thus more rapid than the cellular growth rates and the dynamic changes in the microorganism's environment (Varma and Palsson, 1994). Accordingly, the FBA assumes that metabolic fluxes are in a quasi-steady state relative to growth and process transients. Fig. 1A presents a generalizes concept of FBA, where the observed consumption rate and the objective function (Z) criteria (to maximize/minimize of the rate a specific reaction) are used to find the rate values of rest of network's reaction. A more detailed description of SMN modelling and FBA can be found in Oberhardt et al. (2009) and Orth et al. (2010).

2.3. Model calibration

Calibration of the metabolic network was performed to estimate the stoichiometric coefficients of reactions by minimizing the average normalized root square of errors (nRSE) (Eq. (S1) and Eq. (S2) of SI) between model predictions and reported values of 17 yield ratios (Table 1) for *N. europaea* metabolism under unlimited electron donor (NH_4^+) and acceptor (O_2). Results of model's FBA simulations were applied in the equations presented in Table S4 of SI to estimate the 17 yield ratios. Estimations of the 17 yield rations were performed repeatedly using different model's variants until reach the minimum average nRSE score. Details to the calibration procedure can be found in the section S2 of SI.

Maximizing biomass production as the objective function has been reported to give accurate estimates of cellular phenotypes (Orth et al., 2010; Schuetz et al., 2007); however, to confirm this we evaluate various objective functions involving maximization of biomass production ($Z=v_{Biomass-Synt}$), electrons produced by HAO reaction ($Z=v_{HAO-hno2}$), ATP synthesis ($Z=v_{ATP-Synt}$), electron equivalents production by cytochrome bc1 ($Z=v_{Cytbc1}$), NO_2^- detoxification through *NIR* reaction ($Z=v_{NIR}$), and periplasmic proton potential by cytochrome aa3 ($Z=v_{Cytaa3}$). The best fitting objective function was the one that gave the lowest average nRSE. No further recalibration of the calibrated model was performed for different environmental conditions as a variation in metabolic state only influences the rates of reactions but not reaction stoichiometry (Becker et al., 2007; Orth et al., 2010).

2.4. Regulatory reactions of NO and N_2O production

To assess metabolic regulation of production of NO/N_2O, a sensitivity analysis was performed for the five reactions directly involved in their production – *NO1*, *NIR*, *NOR*, *NO-Ex* and *N_2O-Ex*. A Latin-Hypercube approach was adopted to perform 12,000 simulations using random values between 0 and 1 for specific rates v_j of the reactions involved in consumption of substrates, intracellular pools of electron carriers, and energy production metabolism, along with FBA to estimate the rates of the *NO1*, *NIR*, *NOR*, *NO-Ex* or *N_2O-Ex* reactions. Details of this procedure are presented in section S3 of SI. The reaction sensitivity was assessed by calculating sensitivity coefficients$(S^{\sigma}_{z_i})^2$ using Eq. (S3) in SI (Saltelli et al., 2008).

2.5. Estimating metabolic reactions rates in experiments

The rates of reactions in the metabolic pathways of energy, NO, and N_2O production were estimated from two previous experiments on nitrification by *N. europaea* reported by Yu et al. (2010). The first experiment involved exposing the cell culture in chemostats to oxic–anoxic–oxic transition under a constant influent ammonium concentration of 20 mM during, while the second experiment involved subjecting the cell

Table 1 – Seventeen M yield ratios that describe energy generation metabolism in *N. europaea* operating under non-limiting oxygen and ammonium concentrations and their fitted values and nRSE scores obtained from AOB-SMN model's simulations using different objective functions (Z). Equations to estimate the rate values using the AOB-SMN model are specified in Table S4.

Yield number	Yield ratio	Description of yield ratio	References	Units	Reported value in literature	Estimated rate values (nRSE scores)		
						$Z = \upsilon_{Biomass-Synt}$	$Z = \upsilon_{ATP-Synt}$	$Z = \upsilon_{Cytaa3}$
1	$\frac{O_2}{NH_4^+}$	Overall stoichiometry of ammonium oxidation to nitrite	1, 2	$\frac{mol\ O_2}{mol\ N}$	1.5	1.43 (0.047)	1.43 (0.047)	1.5 (0)
2	$\frac{NO_2^-}{NH_4^+}$	Overall stoichiometry of ammonium oxidation to nitrite	1, 2	$\frac{mol\ N}{mol\ N}$	1	0.99 (0.009)	0.99 (0.009)	1 (0)
3	$\frac{Biomas^{\#}}{NH_4^+}$	Overall stoichiometry of ammonium oxidation to nitrite	1, 2, 3	$\frac{mol\ N}{mol\ N}$	0.012	0.0095 (0.205)	0.0095 (0.205)	0 (1)
4	$\frac{H_2O}{NH_4^+}$	Overall stoichiometry of ammonium oxidation to nitrite	1, 2,	$\frac{mol\ H_2O}{mol\ N}$	1	1.088 (0.088)	1.088 (0.088)	1 (0)
5	$\frac{NO_2^-}{NH_4^+}$	Overall stoichiometry of ammonium oxidation to nitrite	3	$\frac{mol\ N}{mol\ N}$	0.011	0.010 (0.37)	0.010 (0.37)	0 (1)
6	$\frac{ATP_{Biomass}}{ATP_{Synthetized}}$	Growth associated ATP consumption	2, 3, 4	$\frac{mol\ ATP}{mol\ ATP}$	0.35	0.357 (0.021)	0.357 (0.021)	NA
7	$\frac{ATP_{Manteinance}}{ATP_{Synthetized}}$	Maintenance associated ATP consumption	4	$\frac{mol\ ATP}{mol\ ATP}$	0.65	0.643 (0.011)	0.643 (0.011)	NA
8	$\frac{\rightarrow H^+}{NH_4^+}$	Total protons translocated per mol of ammonium oxidised	3, 5	$\frac{mol\ H}{mol\ N}$	9	8.54 (0.051)	8.54 (0.051)	9 (0)
9	$\frac{\rightarrow H^+}{NH_2OH}$	Total protons translocated per mol of hydroxylamine oxidised	3, 5	$\frac{mol\ H}{mol\ N}$	8	7.54 (0.057)	7.54 (0.057)	8 (0)
10	$\frac{\rightarrow H^+}{NH_4^+ * O}$	H^+/O yield from ammonium oxidation	5	$\frac{mol\ H}{mol\ O}$	3.4	6 (0.764)	6 (0.764)	3 (0.765)
11	$\frac{\rightarrow H^+}{NH_2OH * O}$	H^+/O yield from hydroxylamine oxidation	5	$\frac{mol\ H}{mol\ O}$	4.4	4 (0.090)	4 (0.090)	3 (0.091)
12	$\frac{O_{2AMO}}{O_2}$	Oxygen consumption ratio by AMO reaction	6	$\frac{mol\ O_2}{mol\ O_2}$	0.66	0.69 (0.0411)	0.69 (0.0411)	0.67 (0.001)
13	$\frac{O_{2Cytaa3}}{O_2}$	Oxygen consumption ratio by *Cytaa3* reaction	6	$\frac{mol\ O_2}{mol\ O_2}$	0.33	0.31 (0.079)	0.31 (0.079)	0.33 (0.001)
14	$\frac{H^+_{Leaked}}{\rightarrow H^+}$	Proton gradient dissipation not associated to ATP production	3	$\frac{mol\ H}{mol\ H}$	4.5	2.28 (0.493)	2.28 (0.493)	0 (1)
15	$\frac{Q8H_2\ used\ by\ AMO}{Q8H_2\ Synthetized}$	Ubiquinol-8 (q8h2) oxidation ratio by AMO reaction	7	$\frac{mol\ Q8H_2}{mol\ Q8H_2}$	0.5	0.51 (0.02)	0.51 (0.02)	0.5 (0.000)
16	$\frac{Q8H_2\ used\ by\ Cytbc1}{Q8H_2\ Synthetized}$	Ubiquinol-8 oxidation ratio by Cytochrome bc1 reaction	7	$\frac{mol\ Q8H_2}{mol\ Q8H_2}$	0.4125	0.442 (0.02)	0.442 (0.02)	0.5 (0.214)
17	$\frac{Q8H_2\ used\ by\ NADHSynt}{Q8H_2\ Synthetized}$	Ubiquinol-8 oxidation ratio by NADH synthesis reaction	7	$\frac{mol\ Q8H_2}{mol\ Q8H_2}$	0.08754	0.058 (0.22)	0.058 (0.22)	0 (1)
	Average nRSE (% of error)					0.152^A	0.152^A	0.338^B

References: 1 = Grady et al. (1999), 2 = Tchobanoglous et al. (2003), 3 = Poughon et al. (2001), 4 = Vadivelu et al. (2006), 5 = Hollocher et al. (1982) 6 = Ni et al. (2011), 7 = Whittaker et al. (2000).

[#] Biomass as a molecule with the standard formula $C_5H_7O_2N$.

NA = A flux is not available to estimate yield ratio.

[A] or [B] = Values detonated with different letters differ significantly according to one way ANOVA test at $P < 0.05$.

culture to the transition with the influent ammonium concentration maintained at 20 mM during the oxic periods but lowered from 20 mM to 10 mM during the anoxic period. Both experiments were conducted in bioreactors with 4 L of working volume using $2.4 \pm 0.5 \times 10^8$ cells/mL of *N. europaea* during the entire experiment. The experimental rates of production of nitrogenous compounds observed at different instants of time were used as model's input and calibration data as described below.

The experimental rates were estimated by splitting the concentration curves for nitrogenous compounds over the 135 h duration into 135 hourly intervals. The metabolic compounds were assumed to be at pseudo-steady state in each interval (Mahadevan et al., 2002), giving 135 point values for the concentrations of nitrogenous compounds in bioreactor. These values were used along with the influent concentrations and the aqueous flow rate to chemostat in eqn. S4 of SI (as described in section S4.1 of SI) to obtain rates for each compound over the 135 hourly intervals. The metabolic reaction rates were estimated by performing135 FBA simulations for each experiment by specifying the observed ammonium consumption rate to the NH_4-*Ex* reaction over each interval. In each FBA simulation, the rate value υ_{Cytaa3} of the terminal oxidase (*Cytaa3*) was specified to fit the observed

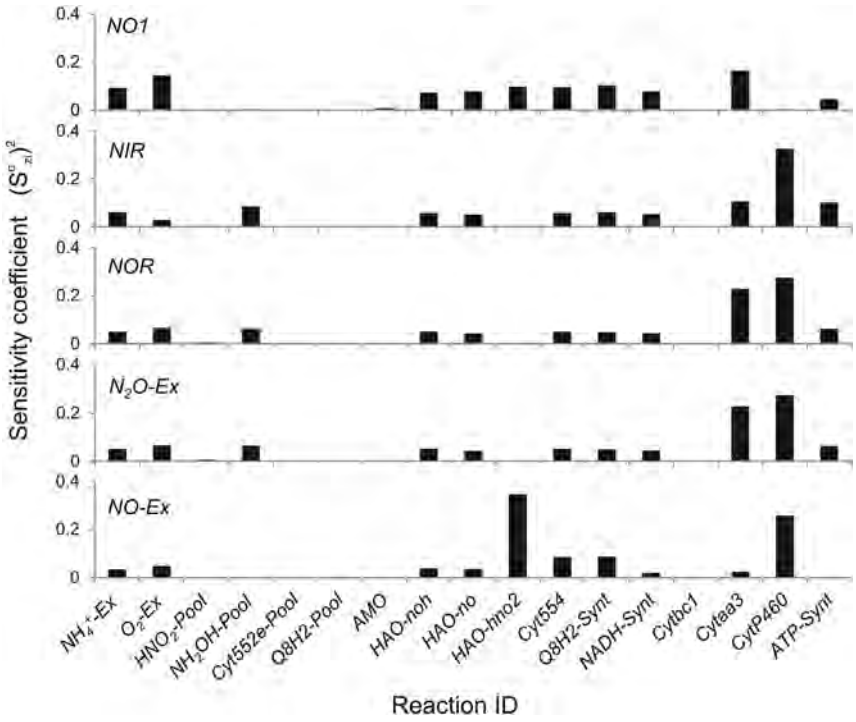

Fig. 2 – Five independent sensitivity analyses of *NO1*, *NIR*, *NOR*, *N_2O-Ex* and *NO-Ex* reactions. The sensitivity coefficients of each analysis were obtained from randomly and independently constrained 17 reactions (X axis) in the AOB-SMN model.

rate of N_2O production; in a similar way the rate value $\upsilon_{HAO-hno2}$ of hydroxylamine oxidoreductase (*HAO-hno2*) reaction was specified to fit the observed rate of NO production. The maximum rate values $\beta_{CytP460} = 0.037$ mmol/h and $\beta_{NO1} = 0.05$ mmol/h were used in all 135 FBA simulations in accordance with the maximum rate values for cytochrome P460 and HAO enzymes reported by Numata et al. (1990) and Sayavedra-Soto and Arp (2011) – details of how these values were obtained are presented in section S4.2 of SI. Finally, the accuracy of the model's estimations was assessed using coefficients of determination (R^2), slope values (m) and root mean square errors (RSME) (Eq. (4) of SI) between experimental and estimated rates of production of NO_2^-–N, NO–N, N_2O–N and cell-N (i.e., nitrogen incorporated in biomass).

3. Results

3.1. *Metabolic network calibration*

The objective functions for maximizing biomass production ($Z=\upsilon_{Biomass-Synt}$) and maximizing ATP synthesis ($Z=\upsilon_{ATP-Synt}$) gave the same lowest average nRSE of 0.152 (Table 1), interpreted as a percentage of accuracy of 84.8% (from (1 −ratios, nRSE)*100) to fit the 17 observed yield values. As the estimated molar yields and nRSE values obtained with $Z=\upsilon_{Biomass-Synt}$ and $Z=\upsilon_{ATP-Synt}$ were identical, FBA of *N. europaea* metabolism can be performed using either of these objective functions as biomass synthesis is inherently linked to ATP synthesis. Therefore, consistent with literature (Schuetz et al., 2007; Orth et al., 2010), $Z=\upsilon_{Biomass-Synt}$ was adopted as the objective function for FBA in this study. The stoichiometric equations obtained by calibrating the model (i.e. corresponding to the lowest average nRSE using $Z=\upsilon_{Biomass-Synt}$) are presented in Table S1 of SI. The rates for the energy production metabolism of *N. europaea* operating under non-limiting oxygen and ammonium concentrations, estimated using the calibrated model, are shown in Fig. 4A. According to our calibration AOB take up1.012 mol of nitrogen per mole of NH_3–N oxidized by AMO (mol-N/mol-N_{AMO}). Thus, 1 mol N as NH_3 is oxidized to NH_2OH and 0.012 mol-N are assimilated into cell biomass. In the AMO reaction producing NH_2OH 0.999 mol-N is oxidized to HNO_2 through the *HAO-noh*, *HAO-no* and *HAO-hno2* reactions and 0.001 mol-N 'leaks' as NO via the *NO1* reaction to extracellular space. *CytP460, NIR* and *NOR* reactions remain inactive under non-limiting oxygen and ammonium conditions, and no N_2O is produced. The yield coefficient for nitrogen assimilation into biomass is estimated as 0.012 mol-N/mol-N_{AMO}, consistent with the reported value of 0.15 g-COD/g-N (0.013 mol-N/mol-N_{AMO}) (Grady et al., 1999).

3.2. *Regulatory reactions of NO and N_2O production*

The sensitivity analysis identified the reactions catalysed by the terminal oxidase cytochromes aa3 (*Cytaa3*), the cytochrome P460 (*CytP460*) and the third step of the hydroxylamine oxidation reaction (*HAO-hno2*) as having a prominent mitigation effect on the rates of N_2O and NO exchange and production via reactions *NO-Ex*, *N_2O-Ex*, *NO1*, *NIR*, and *NOR*. Fig. 2 shows the largest sensitivity coefficients $(S^{\sigma}_{z_i})^2$ for *Cytaa3* and *CytP460* reactions obtained in five sensitivity analyses. The sensitivity coefficients of *NO1*, *NIR* and *NOR* reactions

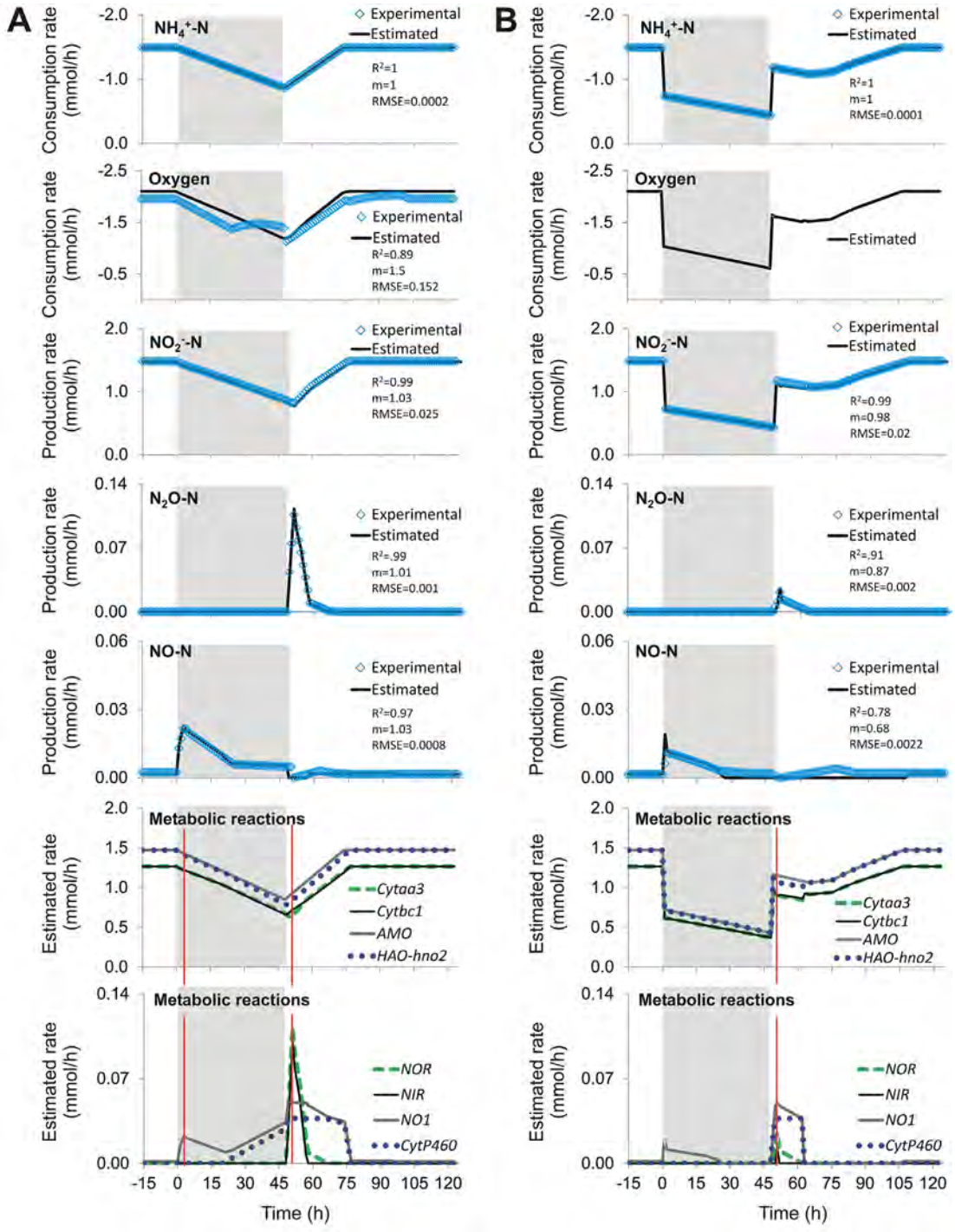

Fig. 3 – Bioreactor's experimental and predicted rates of *N. europaea* nitrification process exposed to oxic–anoxic–oxic transition. In all graphics, the X axis represents time; the anoxic period is shown with grey background and starts at time zero. (A) Oxic–anoxic–oxic transition with non-limiting influent ammonium concentration of 20 mM. (B) Oxic–anoxic–oxic transition with lowered influent ammonium concentration of 10 mM during the anoxic period. Coefficient of determination (R^2), slope (*m*) and root mean square error (RMSE) values between estimated and experimental rates are shown. Vertical lines on the metabolic-reactions graphics indicate the time for which data was analysed in Fig. 4.

indicate that NO/N_2O production by nitrifier denitrification and/or hydroxylamine oxidoreductase mediated pathways is governed by *Cytaa3* and *CytP460* reactions (with $(S^{\sigma}_{z_i})^2$ coefficients ranging between 0.1–0.35), as cytochromes -aa3 and -P460 determine the availability of electrons equivalents (as periplasmic cytochrome 552) for *NIR* and *NOR* (Fig. 1C). Similar sensitivity coefficients for the 17 constrained reactions suggest that N_2O-*Ex* is fully governed by the *NOR* reaction (sub-

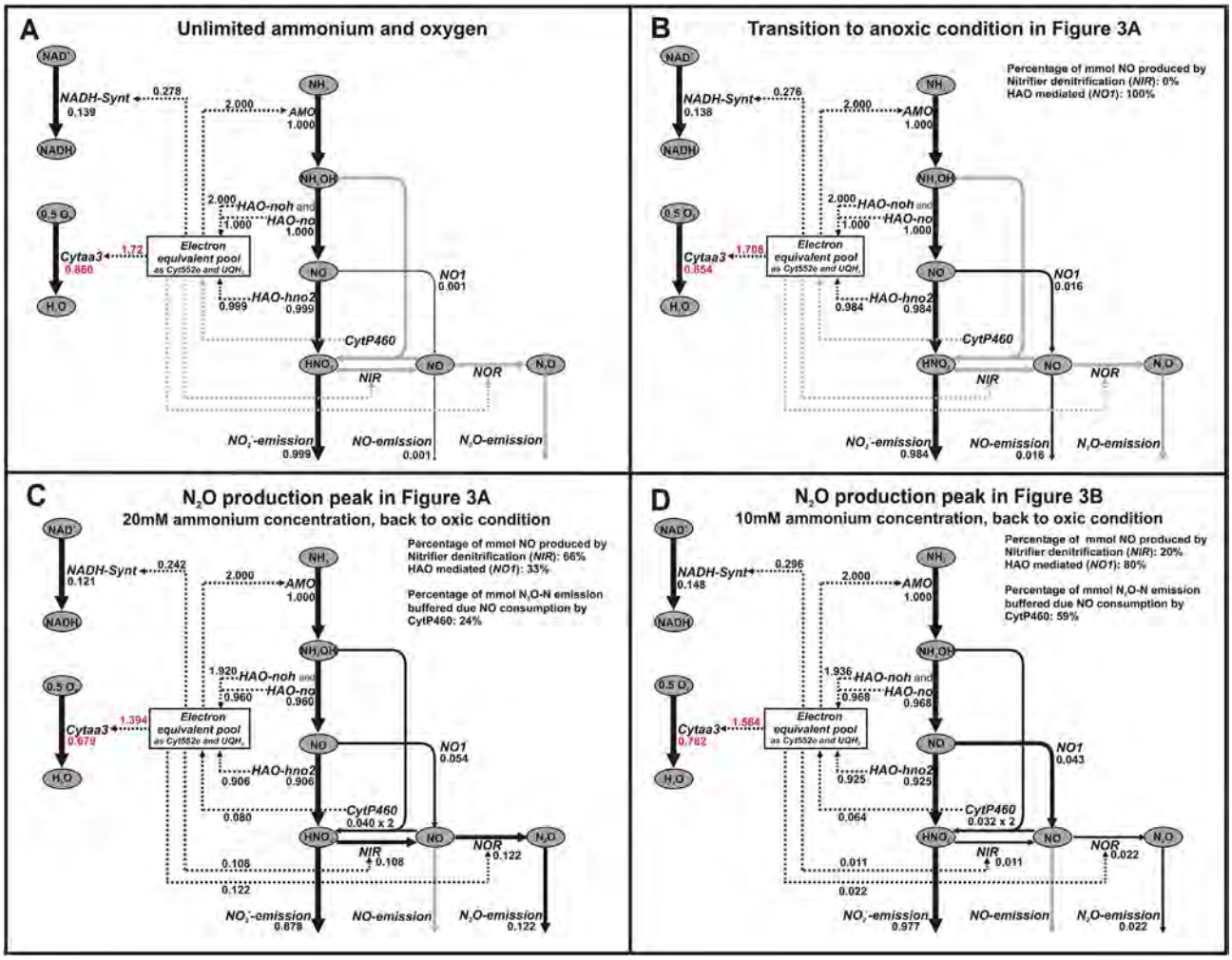

Fig. 4 – Scheme of electron flow through *N. europaea*'s energy and NO/N_2O production pathways along with their estimated rates. Solid lines show the flow of metabolic compounds, while dotted lines represent the flow of electron equivalents. All shown rates were normalized by 1 mmol of NH_3 oxidized by AMO. (A) Unlimited oxygen and ammonium conditions; (B) Transition to anoxic condition with constant ammonium from Fig. 3A; (C) Peak of N_2O production in experiment from Fig. 3A; and (D) Peak of N_2O production in experiment from Fig. 3B.

figures "*NOR*" and "N_2O-*Ex*" of Fig. 2). In contrast, *NO-Ex* was governed by the *CytP460* and *HAO-hno2* reactions but not by *Cytaa3* (sub-figure "*NO-Ex*" of Fig. 2). *NIR*, *NOR* and N_2O-*Ex* reactions showed sensitivity to the rates of consumption of intracellular hydroxylamine with $(S^{\sigma}_{z_i})^2$ values between 0.07 and 0.09 but not to the rates of consumption of intracellular nitrous acid, reduced periplasmic cytochrome 552, and ubiquinol-8 ($(S^{\sigma}_{z_i})^2 = 0$).

3.3. *Metabolic reaction rate estimation from NO/N_2O production experiments*

The R^2, slope (m), and RMSE for observed versus fitted values indicate that the SMN model adequately estimates the rates of production of nitrogenous compounds and metabolic reactions for the experiments reported by Yu et al. (2010) (Fig. 3). The estimated metabolic rates (normalized with the *AMO* reaction rate) under unlimited ammonium and oxygen, and during peak NO and N_2O emission in oxic–anoxic–oxic transition, are shown in Fig. 4. Following the transition to anoxia, NO was emitted via the HAO mediated pathway *NO1* (Figs. 3A and 4B), but only when the rate of *NO1* reaction exceeded that of *CytP460* reaction. At peak N_2O emission following the recovery to oxia the *HAO-hno2* rate was slightly lower than that for *AMO* reaction. Similarly, the *Cytaa3* rate was slightly lower than the *Cytbc1* rate. NO 'leaked' through the *NO1* reaction. Moreover, the coordinated rates for *NOR* and *NIR* reactions at the time of peak N_2O production indicate that 66% of the N_2O emission could be attributed to nitrifier denitrification (Figs. 3A and 4C).

Figs. 3B and 4D show that following the transition to anoxia in the experiment with a lower influent ammonium concentration of 10 mM during the anoxic phase, the *NIR* reaction rate was estimated as zero and entire NO production occurred via the HAO mediated pathway *NO1*. As in previous experiment during recovery following the transition to oxia from anoxia the coordinated rates of *NOR* and *NIR* reactions peak at

the same time as the N_2O emission peak (Fig. 3B), and the maximum *CytP460* rate of 0.037 mmol/h was maintained due to a demand for electron equivalents and the activation of *NO1* pathway. The peak rates for *NOR* and *NIR* of 0.022 and 0.011 mmol/h, respectively, are lower than *NO1* (0.043 mmol/h) and indicate that only 20% of the peak N_2O emission may be attributed to nitrifier denitrification (Fig. 4D).

4. Discussion

4.1. N. europaea *metabolic network for energy and NO/N_2O production*

The reconstruction of NO and N_2O production pathways was based on metabolic reactions experimentally shown to be active in *N. europaea* metabolism (references cited in Table S1 of SI). Alternative NO and N_2O production/consumption reactions such as chemo-denitrification or N_2 production from N_2O (Schmidt, 2008) were not included in the reconstruction as *N. europaea* does not have the genomic potential to perform these reactions. Two reactions catalysed by the cytochromes c′-beta and c554 that could produce N_2O in *N. europaea* (Chandran et al., 2011; Stein, 2010) were ignored as the reactions catalysed by these enzymes use the same substrate and have a similar reaction mechanism to *NOR* (Schmidt, 2008), and due to a lack of sufficient biochemical information on these reactions in the literature. Nitrite and nitrous oxide reductases have cytochrome c oxidoreductase activity and Cyt552e satisfies the mass and charge balances for these reactions (Stein, 2010, 2011); therefore our model uses reduced periplasmic cytochrome 552 (Cyt552e) as the electron donor in *NOR* and *NIR* reactions. In the AOB-SMN model, anabolic pathways such as the Calvin–Benson–Bassham cycle, central carbon reactions and amino acid synthesis were ignored as the rates of production of nitrogenous compounds can be accurately estimated by calibrating the protein and biomass synthesis reactions against experimental biomass yield. As nitrogen assimilation into biomass accounts for less than 2% of total NH_4^+–N consumed by AOB (Tchobanoglous et al., 2003), the maximum error in the nitrogen mass balance by excluding the anabolic reactions is estimated as 2%.

4.2. *Regulatory mechanism of NO and N_2O production*

The model presented here is an investigative tool for deciphering the mechanism of NO/N_2O production by AOB. We report on the activation of N_2O production pathway as a mechanism for dissipating electron equivalents accumulating due to an imbalance in the rates of consumption of electron donor (NH_4^+) and acceptor (O_2). As *N. europaea* is commonly and abundantly found in full scale nitrification processes (Wagner et al., 2002) and that AOB species have a similar N_2O production mechanism (Stein, 2011), the findings of this study are applicable to a wide range of scenarios. Nevertheless, the model developed in this study is a first step in the use of metabolic network modelling to quantify biological pathways of NO/N_2O production in wastewater treatment systems and a more accurate description requires the development of a multispecies model.

The high R^2 and slope, and low RMSE, between the estimated and observed production and consumption rates of nitrogenous compounds (Fig. 3) suggests that NO and N_2O production was accurately modelled and that the estimated intracellular rates appropriately quantify the rates of metabolic reactions. FBA indicates that the activation of *NIR* and *NOR* reactions is a consequence of electron overproduction (as Cyt552e) by *Cytbc1* and *CytP460* relative to the capacity of terminal oxidase *Cytaa3* to use the produced electrons. Electron availability results in activating *NIR* and *NOR* reactions and the consequent production of NO and N_2O. This overproduction of electrons is the consequence of either a lack of oxygen as the final electron acceptor or an excess of the electron donors NH_4^+ and/or NH_2OH. The *CytP460* reaction buffers against the emission of NO and N_2O by oxidizing NO back to HNO_2. During the anoxic phase *CytP460* activity results from availability of NO and NH_2OH, and because this reaction is energetically favoured in cells as it produces reduced periplasmic cytochrome 552 (Cyt552e). Consequently, *CytP460* served dual roles of NO detoxification and producing electron equivalents as cytochrome c552. Our analysis suggests that NO and N_2O are emitted when the sum of the rates of *NIR* and *NO1* reactions exceeds half the of *CytP460* rate.

The FBA estimates that around 70% of the peak N_2O–N emitted during transition to oxia under non-limiting ammonium concentration could be attributed to nitrifier denitrification (Figs. 3A and 4C). This result agrees with observations in experiments performed under similar conditions on the fraction of N_2O produced through nitrifier denitrification (Wunderlin et al., 2013) and increased *nirK* gene expression (Yu et al., 2010). For the experiment with lowered ammonium concentration during the anoxic phase, only 0–20% of N_2O production during transition to oxia could be attributed to nitrifier denitrification while the rest resulted from the *NO1* pathway (Figs. 3B and 4D). This is attributed to the electron equivalents generated by cytochromes bc1 and P460 as being insufficient to activate the *NIR* reaction, consistent with observations during the recovery period of decreased *nirK* gene expression compared to the experiment with elevated ammonium concentration (Yu et al., 2010). In similar experiments involving the use of isotope signatures, all emitted N_2O was attributed to production via the HAO mediated pathway (Wunderlin et al., 2013). Thus, it is possible that N_2O can be produced without involving the *NIR* reaction. However, Fig. 4B suggests that net N_2O emission under this scenario would be expected to be small. FBA of the anoxic phases receiving 20 mM and 10 mM influent ammonium concentrations gave zero rates for the *NIR* reaction and NO production via the *NO1* pathway for both cases (Fig. 4A and B). While these findings contradict observations of increased *nirK* gene expression in *N. europaea* during anoxia (Yu et al., 2010), the FBA indicates that increased *nirK* expression may not have been accompanied with an increase of NIR protein catalytic activity.

5. Conclusions

This study uses stoichiometric network modelling with flux balance analysis to improve the understanding of NO and N_2O

production by biological processes. The key research findings of the study are:

- The regulatory mechanism of NO and N_2O production pathways is related to an imbalance between production and consumption of electron equivalents caused by changes in the environmental availability of electron donors and acceptors.
- The transition to anoxic conditions results in a leak of NO from HAO mediated reaction due to limited availability of electron acceptors to completely oxidize NO to HNO_2.
- The unlimited availability of electron donors combined with a lack of electron acceptors triggers nitrifier denitrification as an electron sink pathway. When electron donor depletion is accompanied with a decrease in electron acceptor concentration so that the intracellular electron equivalents generated are not enough to activate nitrifier denitrification pathway, NO/N_2O production through the hydroxylamine oxidoreductase pathway can be expected.
- The transition from anoxic to oxic conditions causes baseline N_2O production via the hydroxylamine oxidoreductase pathway, but the amount of N_2O emission is dependent upon activation of the nitrifier denitrification pathway.
- NO and N_2O emissions are partially mitigated by the reaction catalysed by cytochrome P460.

Acknowledgements

OP-G was supported by scholarships from The University of Auckland and The Mexican National Council for Science and Technology (CONACyT). OP-G thanks Dr. Diana Spratt Casas for editorial improvement.

Appendix A. Supplementary data

Supplementary data related to this article can be found at http://dx.doi.org/10.1016/j.watres.2014.04.049.

REFERENCES

Ahn, J.H., Kim, S., Park, H., Rahm, B., Pagilla, K., Chandran, K., 2010. N_2O emissions from activated sludge processes, 2008–2009: results of a national monitoring survey in the United States. Environ. Sci. Technol. 44 (12), 4505–4511.

Becker, S.A., Feist, A.M., Mo, M.L., Hannum, G., Palsson, B.Ø., Herrgard, M.J., 2007. Quantitative prediction of cellular metabolism with constraint-based models: the COBRA toolbox. Nat. Protoc. 2 (3), 727–738.

Cabail, M.Z., Pacheco, A.A., 2003. Selective one-electron reduction of *Nitrosomonas europaea* hydroxylamine oxidoreductase with nitric oxide. Inorg. Chem. 42 (2), 270–272.

Chain, P., Lamerdin, J., Larimer, F., Regala, W., Lao, V., Land, M., Hauser, L., Hooper, A., Klotz, M., Norton, J., Sayavedra-Soto, L., Arciero, D., Hommes, N., Whittaker, M., Arp, D., 2003. Complete genome sequence of the ammonia-oxidizing bacterium and obligate chemolithoautotroph *Nitrosomonas europaea*. J. Bacteriol. 185 (9), 2759–2773.

Chandran, K., Stein, L.Y., Klotz, M.G., Van Loosdrecht, M.C.M., 2011. Nitrous oxide production by lithotrophic ammonia-oxidizing bacteria and implications for engineered nitrogen-removal systems. Biochem. Soc. Trans. 39 (6), 1832–1837.

Durot, M., Bourguignon, P., Schachter, V., 2009. Genome-scale models of bacterial metabolism: reconstruction and applications. FEMS Microbiol. Rev. 33 (1), 164–190.

Foley, J., de Haas, D., Yuan, Z., Lant, P., 2010. Nitrous oxide generation in full-scale biological nutrient removal wastewater treatment plants. Water Res. 44 (3), 831–844.

Grady, C.P.L.J., Daugger, G.T., Lim, H.C., 1999. Biological Wastewater Treatment. Marcel Dekker, New York.

Hollocher, T.C., Kumar, S., Nicholas, D.J.D., 1982. Respiration-dependent proton translocation in *Nitrosomonas europaea* and its apparent absence in *Nitrobacter agilis* during inorganic oxidations. J. Bacteriol. 149 (3), 1013–1020.

Kampschreur, M.J., Temmink, H., Kleerebezem, R., Jetten, M.S.M., van Loosdrecht, M.C.M., 2009. Nitrous oxide emission during wastewater treatment. Water Res. 43 (17), 4093–4103.

Kampschreur, M.J., Tan, N.C.G., Kleerebezem, R., Picioreanu, C., Jetten, M.S.M., Van Loosdrecht, M.C.M., 2008. Effect of dynamic process conditions on nitrogen oxides emission from a nitrifying culture. Environ. Sci. Technol. 42 (2), 429–435.

Kampschreur, M.J., Picioreanu, C., Tan, N., Kleerebezem, R., Jetten, M.S.M., Van Loosdrecht, M.C.M., 2007. Unraveling the source of nitric oxide emission during nitrification. Water Environ. Res. 79 (13), 2499–2509.

Kostera, J., Youngblut, M.D., Slosarczyk, J.M., Pacheco, A.A., 2008. Kinetic and product distribution analysis of NO• reductase activity in *Nitrosomonas europaea* hydroxylamine oxidoreductase. J. Biol. Inorg. Chem. 13 (7), 1073–1083.

Mahadevan, R., Edwards, J.S., Doyle, F.J., 2002. Dynamic flux balance analysis of diauxic growth in *Escherichia coli*. Biophys. J. 83 (3), 1331.

Ni, B.-J., Yuan, Z., Chandran, K., Vanrolleghem, P.A., Murthy, S., 2013. Evaluating four mathematical models for nitrous oxide production by autotrophic ammonia-oxidizing bacteria. Biotechnol. Bioeng. 110 (1), 153–163.

Ni, B.-J., Ruscalleda, M., Pellicer-Nàcher, C., Smets, B.F., 2011. Modeling nitrous oxide production during biological nitrogen removal via nitrification and denitrification: extensions to the general ASM models. Environ. Sci. Technol. 45 (18), 7768–7776.

Numata, M., Saito, T., Yamazaki, T., Fukumori, Y., Yamanaka, T., 1990. Cytochrome P-460 of *Nitrosomonas europaea*: further purification and further characterization. J. Biochem. 108 (6), 1016–1021.

Oberhardt, M.A., Chavali, A.K., Papin, J.A., 2009. Flux balance analysis: interrogating genome-scale metabolic networks. Methods Mol. Biol. 500 (1), 61–80.

Orth, J.D., Thiele, I., Palsson, B.O., 2010. What is flux balance analysis? Nat. Biotechnol. 28 (3), 245–248.

Pan, Y., Ni, B.-J., Yuan, Z., 2013. Modeling electron competition among nitrogen oxides reduction and N_2O accumulation in denitrification. Environ. Sci. Technol. 47 (19), 11083–11091.

Poughon, L., Dussap, C.-G., Gros, J.-B., 2001. Energy model and metabolic flux analysis for autotrophic nitrifiers. Biotechnol. Bioeng. 72 (4), 416–433.

Ravishankara, A.R., Daniel, J.S., Portmann, R.W., 2009. Nitrous oxide (N_2O): the dominant ozone-depleting substance emitted in the 21st century. Science 326 (5949), 123–125.

Saltelli, A., Ratto, M., Andres, T., Campolongo, F., Carboni, J., Gatelli, D., Saisana, M., Tarantola, S., 2008. Global Sensitivity Analysis. The Primer. Johon Wiley and Sons, Ltd, West Sussex, England.

Savinell, J.M., Palsson, B.O., 1992. Optimal selection of metabolic fluxes for in vivo measurement. I. Development of mathematical methods. J. Theor. Biol. 155 (2), 201–214.

Sayavedra-Soto, L.A., Arp, D.J., 2011. Ammonia-oxidizing bacteria: their biochemistry and molecular biology. In: Ward, B.B., Arp, D.J., Klotn, M.G. (Eds.), Nitrification. ASM Press, Washington, DC, p. 11.

Schellenberger, J., Que, R., Fleming, R.M.T., Thiele, I., Orth, J.D., Feist, A.M., Zielinski, D.C., Bordbar, A., Lewis, N.E., Rahmanian, S., Kang, J., Hyduke, D.R., Palsson, B.Ø., 2011. Quantitative prediction of cellular metabolism with constraint-based models: the COBRA Toolbox v2.0. Nat. Protoc. 6 (9), 1290–1307.

Schmidt, I., 2008. Nitric oxide: interaction with the ammonia monooxygenase and regulation of metabolic activities in ammonia oxidizers. Methods Enzym. 440, 121–135.

Schuetz, R., Kuepfer, L., Sauer, U., 2007. Systematic evaluation of objective functions for predicting intracellular fluxes in *Escherichia coli*. Mol. Syst. Biol. 3.

Stein, L.Y., 2011. Heterotrophic nitrification and nitrifier denitrification. In: Ward, B.B., Arp, D.J., Klotn, M.G. (Eds.), Nitrification. ASM Press, Washington, DC, p. 95.

Stein, L.Y., 2010. Surveying N_2O-producing pathways in bacteria. Methods Enzym. 486 (C), 131–152.

Tchobanoglous, G., Burton, F.L., Stensel, H.D., 2003. Wastewater Engineering. Treatment and Reuse. Mc Graw Hill, New York.

Thiele, I., Palsson, B.Ø., 2010. A protocol for generating a high-quality genome-scale metabolic reconstruction. Nat. Protoc. 5 (1), 93–121.

Vadivelu, V.M., Keller, J., Yuan, Z., 2006. Stoichiometric and kinetic characterisation of *Nitrosomonas* sp. in mixed culture by decoupling the growth and energy generation processes. J. Biotechnol. 126 (3), 342–356.

Varma, A., Palsson, B.O., 1994. Metabolic flux balancing: basic concepts, scientific and practical use. Bio/Technol. 12 (10), 994–998.

Wagner, M., Loy, A., Nogueira, R., Purkhold, U., Lee, N., Daims, H., 2002. Microbial community composition and function in wastewater treatment plants. Antonie van Leeuwenhoek. Int. J. General. Mol. Microbiol. 81 (1–4), 665–680.

Whittaker, M., Bergmann, D., Arciero, D., Hooper, A.B., 2000. Electron transfer during the oxidation of ammonia by the chemolithotrophic bacterium *Nitrosomonas europaea*. Biochim. Biophys. Acta – Bioenerg. 1459 (2–3), 346–355.

Wuebbles, D.J., 2009. Nitrous oxide: no laughing matter. Science 326 (5949), 56–57.

Wunderlin, P., Lehmann, M.F., Siegrist, H., Tuzson, B., Joss, A., Emmenegger, L., Mohn, J., 2013. Isotope signatures of N_2O in a mixed microbial population system: constraints on N_2O producing pathways in wastewater treatment. Environ. Sci. Technol. 47 (3), 1339–1348.

Wunderlin, P., Mohn, J., Joss, A., Emmenegger, L., Siegrist, H., 2012. Mechanisms of N_2O production in biological wastewater treatment under nitrifying and denitrifying conditions. Water Res. 46 (4), 1027–1037.

Yu, R., Kampschreur, M.J., Van Loosdrecht, M.C.M., Chandran, K., 2010. Mechanisms and specific directionality of autotrophic nitrous oxide and nitric oxide generation during transient anoxia. Environ. Sci. Technol. 44 (4), 1313–1319.